Comparative ESR and Catalytic Studies of Ethylene Dimerization on Pd(II)-Exchanged Clinoptilolite, Mordenite, Ferrierite, and SUZ-4

Hosun Choo,[†] Suk Bong Hong,[‡] and Larry Kevan*[,†]

Department of Chemistry, University of Houston, Houston, Texas 77204-5641, and Department of Chemical Technology, Taejon National University of Technology, Taejon 303-719, Korea

Received: March 5, 2001; In Final Form: June 7, 2001

Catalytic activity for ethylene dimerization is studied in four palladium-exchanged zeolites, PdH-clinoptilolite, PdH-mordenite, PdH-ferrierite, and PdHK-SUZ-4, with different channel systems. The formation and adsorbate interactions of Pd(I) are also investigated for a better understanding of the role of Pd(I) on the catalytic reaction in these zeolites using electron spin resonance (ESR) spectroscopy. Thermal and hydrogen reduction of Pd(II) in clinoptilolite, mordenite, ferrierite, and SUZ-4 produce isolated Pd(I) with somewhat different ESR parameters. The interaction of Pd(I) with various sizes of adsorbates shows some similarities in PdH-mordenite and PdH-ferrierite, indicating that Pd(I) is located in the main 12-ring and 10-ring channels of mordenite and ferrierite, respectively, where all the Pd(I) can coordinate with methanol and pyridine. However, SUZ-4 shows a noticeable difference in the way Pd(I) interacts with several adsorbates such as ammonia, methanol, and ethylene. These adsorbates reduce Pd(II) to Pd(I) at 298 K, leading to the formation of two Pd(I) ions situated at two different sites of SUZ-4. One is the same Pd(I) ion site formed by thermal reduction but it appears at higher intensity upon adsorption. The other Pd(I) is an isolated Pd(I) produced only after prolonged annealing with adsorbates. Our ESR and catalytic results show that Pd(I) is active for ethylene dimerization in these four channel-type zeolites. This activity is dependent on the location and accessibility of Pd(I) and the reaction temperature. All catalysts deactivate due to the further reduction of Pd(I) by ethylene and butene. Analysis of the composition of butene products indicates that PdH-clinoptilolite and PdHK-SUZ-4 reach a thermal equilibrium distribution faster than do PdH-mordenite and PdH-ferrierite.

Introduction

Molecular sieves with different structures and pore sizes show very interesting shape-selectivity and catalytic activity in several catalytic reactions.[1,2] The active sites of these materials can be prepared by incorporation of transition metal ions into either extraframework or framework sites.[3] These catalytic properties of the transition metal ion modified molecular sieves are dependent on the type, amount, and location of the active transition metal ion. The studies probing the nature and local environment of the transition metal such as Pd(I) and Ni(I) have been accomplished in several zeolite and silicoaluminophosphate (SAPO) materials.[4−10] Palladium-exchanged X and Y zeolites and SAPO materials have been found to exhibit high catalytic activities for ethylene dimerization.[11−13] Electron spin resonance (ESR) and electron spin echo modulation (ESEM) data indicated that Pd(I) is initially coordinated with one molecule of ethylene upon adsorption of ethylene and that this complex is converted into a Pd(I)−$(C_4H_8)_n$ complex, implying that monovalent palladium is catalytically active for ethylene dimerization. The catalytic activity and selectivity of these materials were different depending on the structure and pore size of the supporting materials, the location of Pd(I), and the reaction temperature.[13]

In the past, ESR and ESEM spectroscopies were employed to obtain the information about the location of Pd(I) and its local environment in PdH-clinoptilolite, which is necessary for application of this Pd-exchanged clinoptilolite in catalytic reactions.[14] Thermal reduction of PdH-clinoptilolite produced a single isolated Pd(I) ($g_1 = 2.927$, $g_2 = 2.168$, and $g_3 = 2.136$) in the clinoptilolite structure where Pd(I) was located at a site which was not accessible to the molecules as large as pyridine but was readily coordinated with adsorbates such as ammonia, methanol, and ethylene. Adsorption of ethylene on thermally reduced Pd(I)H-clinoptilolite at room temperature led to the formation of three new ESR species due to the interaction of Pd(I) with ethylene. The ESEM data confirmed the formation of two Pd(I)−$(C_2D_4)_1$ complexes. These species retained almost the same intensities upon annealing, even at 353 K overnight. These ESR and ESEM results, as well as the high ion-exchange capacity and thermal stability of clinoptilolite, prompt us to investigate the catalytic properties of PdH-clinoptilolite in ethylene dimerization.

Like clinoptilolite, mordenite and ferrierite are naturally-occurring silica-rich aluminosilicates with channel systems.[15] They differ in their Si/Al ratios and the channel dimensions, which may influence the accessibility of cations to adsorbates. Their structures are illustrated in Figures 1−3.[16] While clinoptilolite has a two-dimensional interconnecting channel system with one 10-ring channel and two 8-ring channels,[17] mordenite has a one-dimensional, 12-ring channel system with side pockets involving 8-ring channels.[18] The structure of ferrierite is also defined by a two-dimensional channel system with spherical cages. This channel system consists of 10-ring channels intersecting perpendicularly with 8-ring channels.[19]

SUZ-4 is a new synthetic zeolite whose framework consists of 5-rings, 6-rings, 8-rings, and 10-rings.[20] The framework

* Author to whom correspondence should be addressed.
[†] University of Houston.
[‡] Taejon National University of Technology.

10.1021/jp0108420 CCC: $20.00
Published on Web 07/25/2001

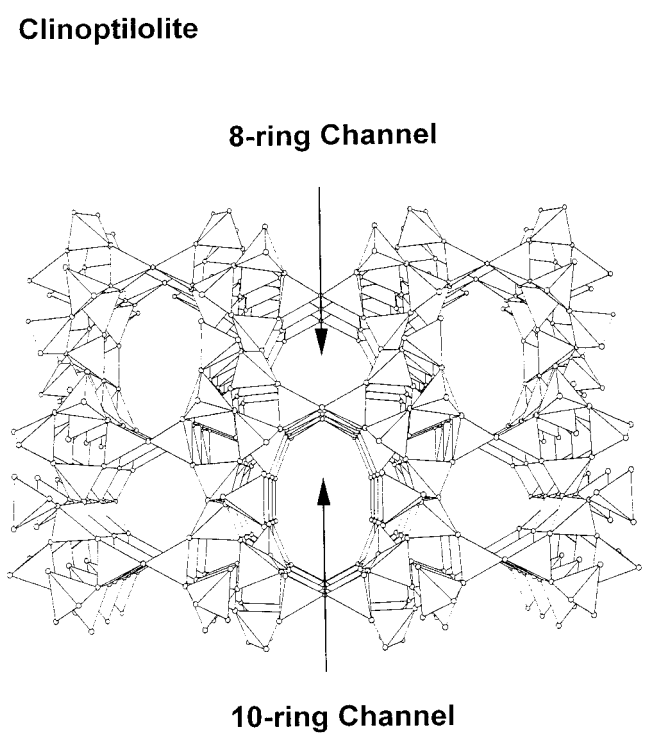

Figure 1. Structural model of clinoptilolite viewed along the *c*-axis. The corner of a tetrahedron represents a framework oxygen. Al and Si atoms are located at the centers of the tetrahedron.

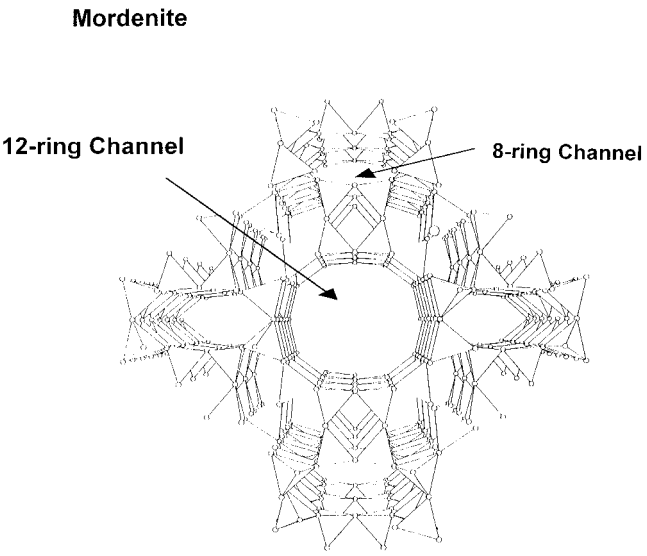

Figure 2. Structural model of mordenite viewed along the *c*-axis. The corner of a tetrahedron represents a framework oxygen. Al and Si atoms are located at the centers of the tetrahedron.

topology of SUZ-4 is related to that of ferrierite. They have the same ab plane projections. The major difference between SUZ-4 and ferrierite is the alignment of chains along the *c*-axis as seen in Figure 4. SUZ-4 has double 6-rings between small cages while ferrierite has single 6-rings between large cages.[21] The structure of SUZ-4 is considered to be a three-dimensional channel system including main straight 10-ring channels intersected by two arrays of 8-ring channels and small cages linked through double 6-rings.[22] The exchangeable potassium ions in HK-SUZ-4 are preferably located in small cages, which are present in SUZ-4 but not in ferrierite.[21,22] The minimum and maximum dimensions of the 10-rings are 4.6 and 5.2 A which are similar to those of ferrierite.

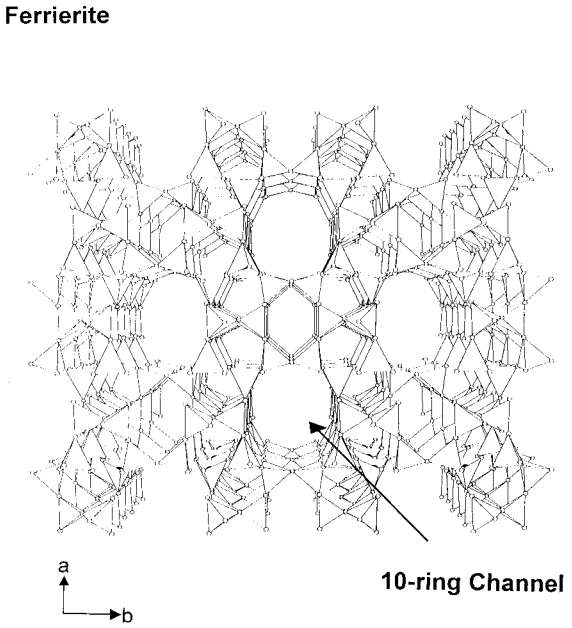

Figure 3. Structural model of ferrierite viewed along the *c*-axis. The corner of a tetrahedron represents a framework oxygen. Al and Si atoms are located at the centers of the tetrahedron.

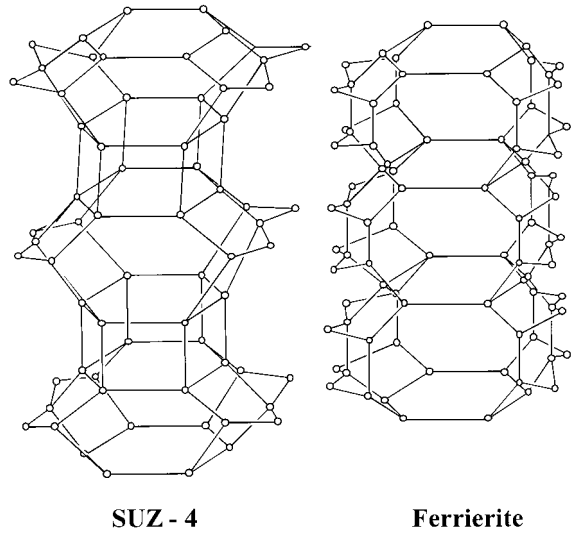

Figure 4. Columns of the unit cell in SUZ-4 and ferrierite along the *c*-axis. Adapted from ref 21.

The present study focuses on these four channel-type zeolites, clinoptilolite, mordenite, ferrierite, and SUZ-4, to see the influence of their characteristic channel systems on the catalytic activity of ethylene dimerization. We report comparative results of ethylene dimerization on Pd-exchanged clinoptilolite, mordenite, ferrierite, and SUZ-4 by using a static reactor and gas chromatography detection of products. We also investigate the formation of Pd(I) and its interactions with various adsorbates in Pd-exchanged H-mordenite, H-ferrierite, and HK-SUZ-4 using ESR to provide a better understanding of the catalytic function of Pd(I) ions in these materials.

Experimental Section

Synthesis. The detailed preparations of NaK-clinoptilolite and NaK-mordenite are described in the cited references.[14,23] They were hydrothermally synthesized without organic templates. Single phase Na-ferrierite[24] and K-SUZ-4[25] were also hydrothermally synthesized as follows. In a typical synthesis of Na-

ferrierite, 0.62 g of NaOH (50% aqueous solution, Aldrich), 0.70 g of $Na_2OAl_2O_3H_2O$ (Strem), and 8.29 g of pyrrolidine (99%, Aldrich) were dissolved into 30 g of deionized water. To this clear solution, 34.62 g of colloidal silica (Ludox AS-40, Dupont) were added. The molar composition of the reaction mixture was 10 R: 1.5 Na_2O: 1.0 Al_2O_3: 30 SiO_2: 370 H_2O where R is pyrrolidine. After stirring at room temperature for 1 day, the final reaction mixture was placed into Teflon-lined 100 mL autoclaves and heated at 448 K for 7 days. After crystallization, the product was washed with water and dried at 343 K overnight. For the synthesis of K-SUZ-4, 0.48 g of $Al(NO_3)_3 \cdot 9H_2O$ (98%, Junsei) and 2.20 g of KOH (45% aqueous solution, Aldrich) were dissolved into 22.01 g of H_2O. To this clear solution, 5.63 g of colloidal silica (Ludox AS-40, Dupont) and 2.48 g of *N*,*N*,*N*′,*N*′,*N*′-hexaethylpentanediammonium (Et_6-diquat-5) dibromide were added. The molar composition of the resulting gel was 4.5 Et_6-diquat-5: 11.0 K_2O: 1.0 Al_2O_3: 30 SiO_2: 1200 H_2O. After stirring at room temperature for 1 day, the final mixture was transferred to 45 mL Teflon-lined autoclaves and heated at 160 °C under slow rotation (60 rpm) for 8 days. The products were recovered by filtration, washed repeatedly with water, and then dried overnight at room temperature. The organic templates trapped within the micropores of the as-synthesized Na ferrierite and K-SUZ-4 were removed by calcination in flowing oxygen at 823 K for 24 h prior to the catalyst testing and ESR measurements.

H-clinoptilolite, H-mordenite, H-ferrierite, and H-SUZ-4 were prepared by liquid-state ion-exchange with 1 M NH_4Cl at 333 K, followed by calcination in flowing air at 773 K for 24 h to remove ammonia. To ensure maximum exchange, this procedure was repeated several times.

The incorporation of Pd(II) into extraframework positions in these materials was achieved by solid-state ion exchange with various amounts of $Pd(NH_3)_4Cl_2 \cdot H_2O$ (Alpha) at 873 K for 24 h.

Sample Treatment and Measurement. Powder X-ray diffraction (XRD) patterns were recorded on a Siemens D5000 X-ray diffractometer using Cu Kα radiation. Chemical analyses of the samples were carried out by electron microprobe analysis on a JEOL JXA-8600 spectrometer. For the various ESR measurements, hydrated samples were loaded into 3 mm o.d. × 2 mm i.d. Suprasil quartz tubes and evacuated at 298 K for 24 h. To study the behavior of Pd(II) as a function of dehydration, the samples were slowly heated under vacuum ($<10^{-4}$ Torr) from room temperature to 373, 473, and 573 K. This procedure accomplishes thermal reduction. To see if any $Pd(I)-(H_2)_n$ complexes are formed during hydrogen reduction, dehydrated samples after the activation process were treated with dry hydrogen at room temperature and subsequently heated to various temperatures from 298 to 673 K for various durations. An activation treatment involved heating dehydrated samples in 500 Torr of dry oxygen at 673 K for 5 h followed by evacuation at the same temperature overnight to reoxidize any Pd(I) formed during dehydration. ESR spectra were then recorded at 77 K to detect the formation of any Pd(I) species. To study Pd(I) interactions with various adsorbates, reduced samples were exposed to the room-temperature vapor pressure of CH_3OD (Stohler Isotope Chemicals), D_2O (Cambridge Isotope), and pyridine (Cambridge Isotopes), 8 Torr of ^{13}CO (Cambridge Isotopes), and 20 Torr of ^{12}CO (Trigas), C_2D_4 (Cambridge Isotopes), C_4H_8 (Trigas), and ND_3 (Stohler Isotope Chemicals). These samples with adsorbates were frozen in liquid nitrogen and sealed for ESR.

The ESR spectra were recorded with a Bruker ESP 300 X-band spectrometer at 77 K. The magnetic field was calibrated with a Varian E-500 gaussmeter. The microwave frequency was measured by a Hewlett-Packard HP 5324A frequency counter.

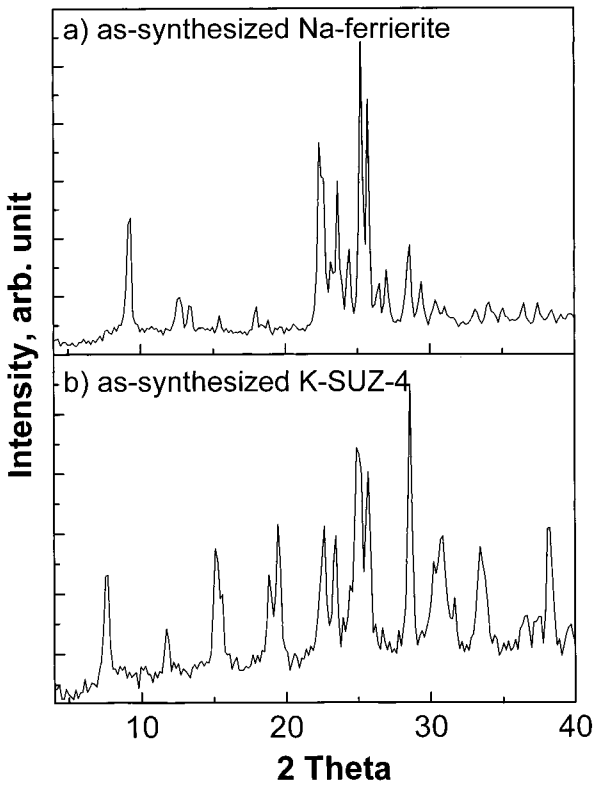

Figure 5. X-ray powder diffraction pattern of as-synthesized (a) Na-ferrierite and (b) K-SUZ-4.

TABLE 1: Elemental Analysis, Si/Al Ratios, and Pd/Al Ratios for PdH-Clinoptilolite, PdH-Mordenite, PdH-Ferrierite, and PdHK-SUZ-4

catalyst	elemental analysis	Si/Al ratio	Pd/Al ratio
PdH-clinoptilolite	$Pd_{0.021}[Si_{0.83}Al_{0.17}]O_2$	4.8	0.12
PdH-mordenite	$Pd_{0.013}[Si_{0.87}Al_{0.13}]O_2$	6.7	0.10
PdH-ferrierite	$Pd_{0.044}[Si_{0.88}Al_{0.12}]O_2$	7.3	0.36
KH-SUZ-4	$K_{0.038}[Si_{0.86}Al_{0.14}]O_2$	6.1	0
PdKH-SUZ-4	$Pd_{0.042}K_{0.024}[Si_{0.86}Al_{0.14}]O_2$	6.1	0.30

Catalyst Testing. A sample of 100 mg was placed on a sintered glass disk inside a glass reactor with a closed, static system of total internal volume of 51 cm^3. The samples reduced as described above were exposed to 100 Torr of ethylene at room temperature and then annealed at 353 K. Reaction products were analyzed at different reaction times by on-line gas chromatography at room temperature with a Varian 3300 gas chromatograph equipped with a thermal conductivity detector. A 7 ft column of 0.085 in i.d. packed with 0.19 wt % picric acid supported on an 80/100 mesh graphic GC support was used. The injection was completed in 5 s.

Results

X-ray Powder Diffraction (XRD). Figure 5 shows the powder XRD patterns of as-synthesized Na-ferrierite and K-SUZ-4. These patterns match, both in intensity and line position, the patterns reported for the corresponding ferrierite and SUZ-4 structures.[23,24] No loss in crystallinity was observed by XRD after as-synthesized ferrierite and SUZ-4 were calcined by heating at 873 K overnight to remove the organic template.

Electron Microprobe Analysis. Table 1 shows the chemical composition of the final ion-exchanged samples estimated by

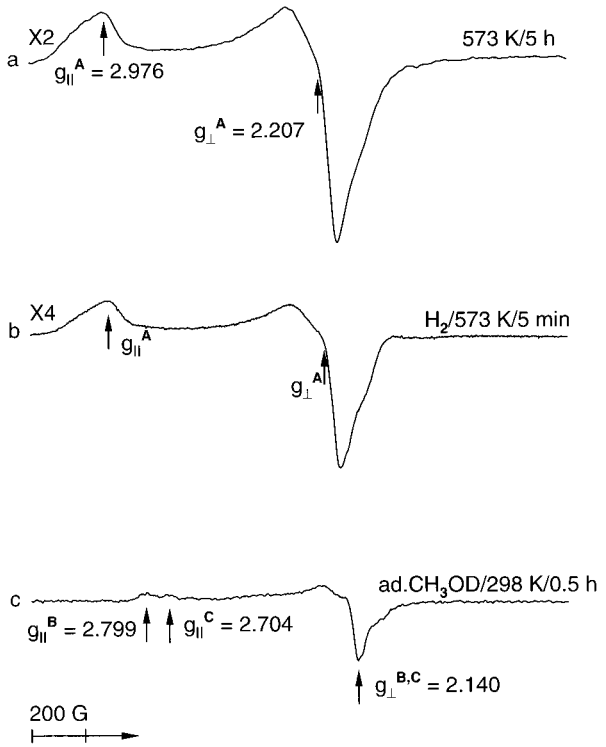

Figure 6. ESR spectra at 77 K of PdH-mordenite after (a) dehydration at 573 K for 5 h, (b) reduction by 20 Torr hydrogen at 573 K for 5 min, and (c) adsorption of 100 Torr CH_3OD on thermally reduced PdH-mordenite at 298 K for 0.5 h.

electron microprobe analysis. It should be noted that significant amounts of potassium ions were not removed in the as-synthesized SUZ-4 even after prolonged ion exchange with 1 M NH_4Cl. This final ion-exchanged sample is designated as HK-SUZ-4.

ESR Measurements. Hydrated samples do not show any ESR signal at 77 K. Thus, the palladium ions exist as Pd(II) which is ESR silent. Figure 6a and 6b shows the ESR spectra of Pd(II)H-mordenite after thermal reduction at 573 K for 5 h and hydrogen reduction at 573 K for 5 min, respectively. Both thermal and hydrogen reduction of PdH-mordenite lead to the formation of a single axial species A with $g_{//}^{A} = 2.976$ and $g_{\perp}^{A} = 2.207$. The ESR signal intensity of this species produced by hydrogen reduction is substantially higher than what was observed after thermal reduction of PdH-mordenite. Species A is assigned to an isolated Pd(I) ion generated by thermal and hydrogen reduction in mordenite. Adsorption of CH_3OD on reduced Pd(I)H-mordenite produces two new species, denoted B and C as can be seen in Figure 6c. They have axial symmetry with different parallel components, $g_{//}^{B} = 2.799$, $g_{//}^{C} = 2.704$, but with the same perpendicular component, $g_{\perp}^{B,C} = 2.140$. These species are assigned to two Pd(I)$-(CH_3OD)_n$ complexes located within the mordenite structure.

Figure 7 shows the ESR spectra of PdH-mordenite after adsorption of ethylene. When 20 Torr of C_2D_4 is adsorbed on a thermally reduced sample at 298 K for 30 min, Pd(I) species A disappears immediately with the formation of two new species, D and E (Figure 7a). Annealing the sample at room temperature and 353 K increases the intensity of species D ($g_{//}^{D} = 2.675$ and $g_{\perp}^{D} = 2.077$). Species D has been reported in Pd-(II)-exchanged H-SAPO-5 and H-SAPO-11 after adsorption of ethylene where this species was assigned to a Pd(I)$-(C_4H_8)_n$ complex based on the ESEM simulation data.[13] The other species *E* ($g_{//}^{E} = 2.419$, and $g_{\perp}E = 2.038$) is dominant immediately after adsorption of ethylene at room temperature

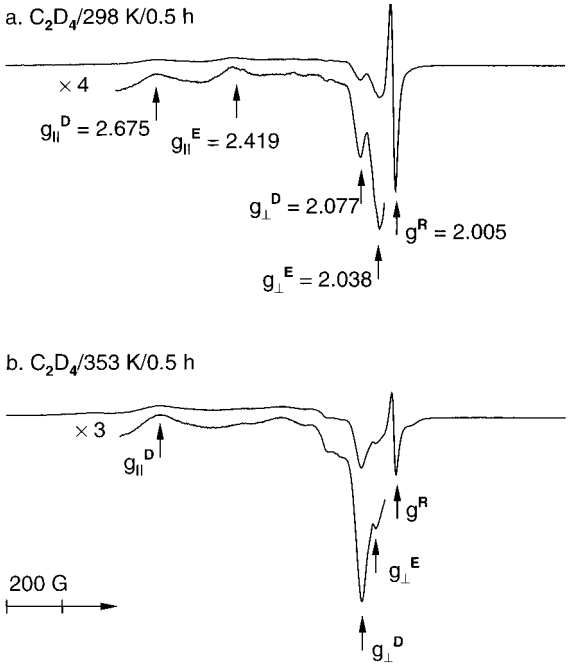

Figure 7. ESR spectra at 77 K of PdH-mordenite after 20 Torr of C_2D_4 adsorption on a thermally reduced sample (a) at 298 K for 0.5 h, and (b) at 353 K for 0.5 h.

but shows a time-dependent decrease in intensity when an ethylene-adsorbed sample anneals at 353 K. This observation suggests that species E is probably due to a Pd(I)$-(C2D4)_n$ complex. Isotropic species R observed along with species D and E has been observed in several other zeolites and SAPO materials where it was tentatively assigned to a free radical species.[26,27]

Figure 8 shows the ESR spectra for Pd(II)H-ferrierite. Dehydration of Pd(II)H-ferrierite at 573 K for 5 h generates single isolated Pd(I) species H with $g_{//}^{H} = 2.645$ and $g_{\perp}^{H} = 2.136$ (Figure 8a). The same species H is also generated with a stronger intensity by hydrogen reduction of PdH-ferrierite at 573 K for 5 min. The *g* values of species H were reported previously for Pd(I) in PdH-SAPO-5,11[7] and PdNaMCM-22[27] and are slightly lower in comparison to Pd(II)-exchanged H-rho zeolite.[28]

Figure 8c and 8d shows the ESR spectra of PdH-ferrierite observed after adsorption of methanol and pyridine, respectively, on thermally reduced Pd(I)H-ferrierite for 30 min. Adsorption of CH_3OD produces a single species, I, with rhombic symmetry; $g_1^{I} = 2.539$, $g_2^{I} = 2.137$, and $g_3^{I} = 2.105$, indicating the formation of a Pd(I)$-(CH_3OD)_n$ complex. Similarly, adsorption of pyridine on reduced Pd(I)H-ferrierite at room temperature for 30 min leads to the formation of a Pd(I)$-(C_5H_5N)_n$ complex ($g_1^{J} = 2.410$, $g_2^{J} = 2.059$, and $g_3^{J} = 2.023$) with unknown isotropic species K ($g^{K} = 2.000$).

The interaction of Pd(I) species H with ethylene in PdH-ferrierite is shown in Figure 9. Adsorption of 20 Torr of ethylene on thermally reduced Pd(I)H-ferrierite at room temperature for 30 min causes Pd(I) species H to disappear immediately and new species L is generated with $g_1^{L} = 2.412$, $g_2^{L} = 2.053$, and $g_3^{L} = 2.019$. This species is assigned to a Pd(I) complex with ethylene since species L decreases with annealing of a sample at 353 K. Figure 9b shows the ESR spectrum observed after ethylene-adsorbed PdH-ferrierite anneals at 353 K for 1.5 h. Two new species, denoted M and N, are observed with $g_{//}^{M} = 2.655$, $g_{//}^{N} = 2.272$, $g_{\perp}^{M} = 2.079$, and $g_{\perp}^{N} = 2.049$. Species M has ESR parameters similar to those of species D already

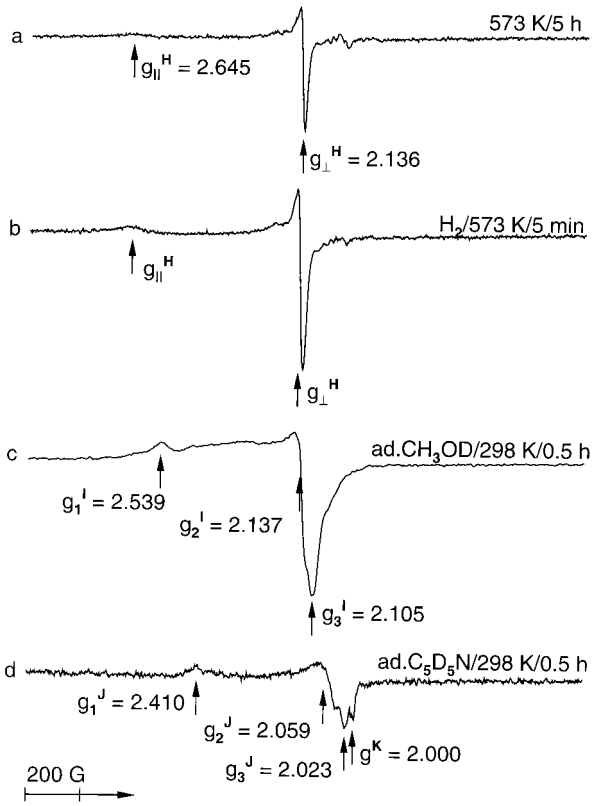

Figure 8. ESR spectra at 77 K of PdH-ferrierite after (a) dehydration at 573 K for 5 h, (b) reduction by 20 Torr hydrogen at 573 K for 5 min, (c) adsorption of 100 Torr CH_3OD at 298 K for 0.5 h, and (d) adsorption of ~20 Torr C_2D_5N at 298 K for 0.5 h.

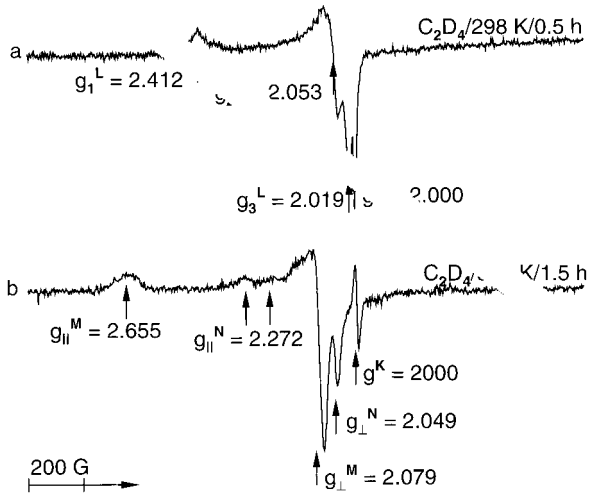

Figure 9. ESR spectra at 77 K of PdH-ferrierite after 20 Torr of C_2D_4 adsorption on a thermally reduced sample at (a) 298 K for 0.5 h, and (b) 353 K for 1.5 h.

assigned to a Pd(I)−$(C_4H_8)_n$ complex in PdH-mordenite. This species M formed in the ferrierite structure is also assigned to a Pd(I)−$(C_4H_8)_n$ complex which is confirmed by adsorption of 1-butene on a thermally reduced sample. The other species N generated along with the Pd(I)−$(C_4H_8)_n$ complex species M, only after annealing at 353 K, is probably due to a Pd(I) complex with butene, the product of ethylene dimerization.

Figure 10a shows the ESR spectrum of PdHK-SUZ-4 obtained after thermal reduction at 573 K for 5 h. A single new species, O, observed with $g_{//}^{O} = 2.668$ and $g_{\perp}^{O} = 2.138$ is assigned to an isolated Pd(I) within the SUZ-4 structure. The

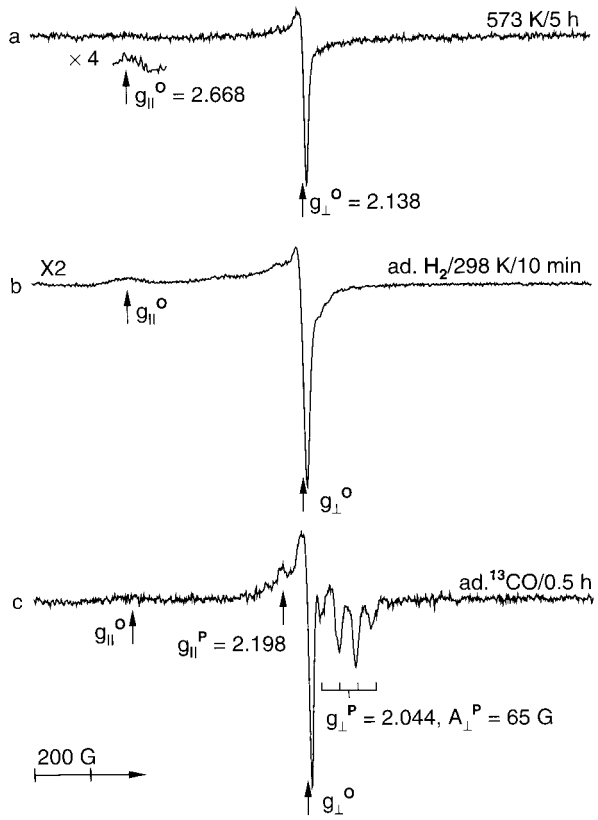

Figure 10. ESR spectra at 77 K of PdHK-SUZ-4 after (a) dehydration at 573 K for 5 h, (b) adsorption of 20 Torr of dry hydrogen for 10 min, and (c) adsorption of 8 Torr of ^{13}CO for 0.5 h on a thermally reduced sample at 298 K.

ESR parameters of Pd(I) species O are similar to those of Pd(I) species H observed in PdH-ferrierite. However, the behavior of Pd(I) with respect to various adsorbates is different between ferrierite and SUZ-4, implying different environments of Pd(I) in these two systems. When 20 Torr of dry hydrogen is adsorbed on thermally reduced Pd(I)HK-SUZ-4 at room temperature for 10 min, species O increases its intensity without forming a Pd(I) complex with hydrogen (Figure 10b). This indicates that adsorbing hydrogen reduces Pd(II) to Pd(I) even at room temperature in SUZ-4.

Adsorption of ^{13}CO on thermally reduced Pd(I)KH-SUZ-4 for 30 min generates new species P with Pd(I) species O still remaining dominant, indicating that only a part of Pd(I) species O is coordinated with carbon monoxide to give new species P ($g_{//}^{P} = 2.198$, $g_{\perp}^{P} = 2.044$) shown in Figure 10c. The ^{13}C hyperfine interaction gives a quartet feature of the $g_{\perp}$ component and $A_{\perp}^{P} = 65$ G. On the basis of the ^{13}C hyperfine structure, species P is assigned to a Pd(I)−$(CO)_3$ complex.

The interaction of Pd(I) species O with ethylene in PdHK-SUZ-4 is different from those observed in PdH-clinoptilolite, -mordenite, and -ferrierite as shown in Figure 11. Adsorption of ethylene on Pd(I)HK-SUZ-4 at 298 K causes Pd(I) species O to increase but does not show any new ESR signal due to the formation of a Pd(I) complex with ethylene. The ESR intensity of Pd(I) species O observed after ethylene adsorption at 298 K for 30 min is nearly 1 order of magnitude higher than that of Pd(I) obtained by thermal reduction. Upon increasing the annealing time or annealing temperature to 353 K, Pd(I) species O becomes more intense with the formation of another new species Q. This new species has a different parallel component ($g_{//}^{Q} = 2.621$) but the same perpendicular component

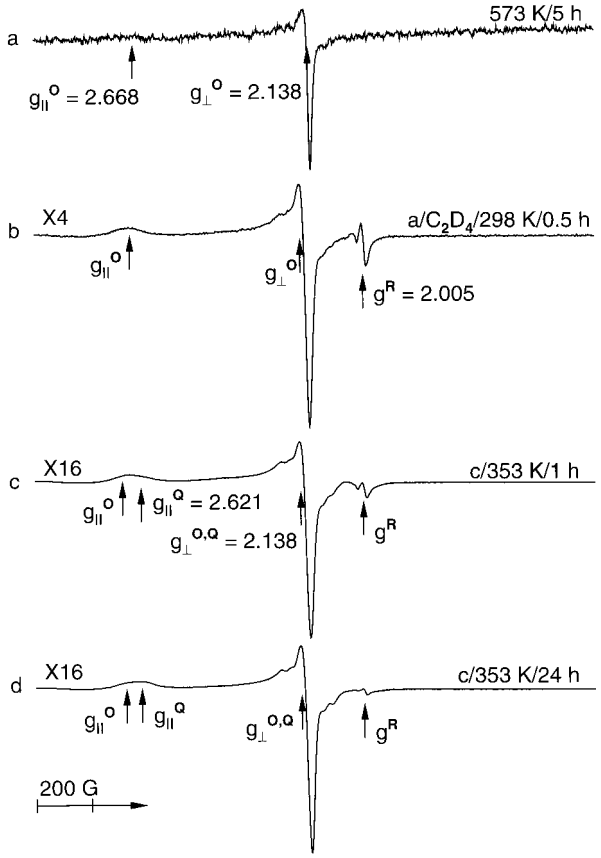

Figure 11. ESR spectra at 77 K of PdHK-SUZ-4 (a) after dehydration at 573 K for 5 h and after adsorption of 20 Torr C_2D_4 on thermally reduced PdHK-SUZ-4 at (b) 298 K for 0.5 h, (c) 353 K for 1 h, and (d) 353 K for 24 h.

($g_{\perp}^{Q} = 2.138$) as that of Pd(I) species O and this species Q becomes dominant as the annealing time increases.

To identify whether this new species Q is another isolated Pd(I) or a Pd(I) complex with ethylene or butene, thermally reduced PdHK-SUZ-4 was exposed to 20 Torr of ammonia and to 100 Torr of methanol. Adsorption of methanol and ammonia on SUZ-4 led to the same ESR spectrum composed of two species O and Q, as that observed after ethylene adsorption (Figure 12). These observations indicate that species Q is probably due to another isolated Pd(I) formed by reduction of Pd(II) by adsorbates and that the two Pd(I) species O and Q are located at two different sites within the SUZ-4 structure.

The changes of spin concentration associated with the adsorption of methanol on thermally reduced PdHK-SUZ-4 at 298 K were compared to those observed after hydrogen adsorption as a function of annealing time. The ESR intensity of Pd(I) species increases as the annealing time increases up to 5 h. From Figure 13 it is also seen that methanol is a much stronger reducing agent than hydrogen at room temperature.

Table 2 summarizes the ESR parameters assigned to the various Pd(I) species observed in PdH-mordenite, PdH-ferrierite, and PdHK-SUZ-4 and their assignments.

Catalyst Testing. Dehydrated H-clinoptilolite, H-mordenite, H-ferrierite, and HK-SUZ-4 show no ethylene dimerization activity. However, PdH-clinoptilolite, PdH-mordenite, PdH-ferrierite, and PdHK-SUZ-4 show catalytic activity for ethylene dimerization when a thermally reduced sample containing Pd(I) is exposed to 100 Torr of ethylene at 298 K and is then annealed at 353 K for various reaction times. This suggests that Pd(I) participates in the formation of active sites. Due to the low Pd(II) concentration and the low turnover, different materials with the same Pd/Al ratio are compared after a reaction time of 24 h. About 20% of the initial ethylene is converted to *n*-butene as in PdH-clinoptilolite (Pd/Al = 0.12) which is higher than the conversion in PdH-mordenite (6% conversion, Pd/Al

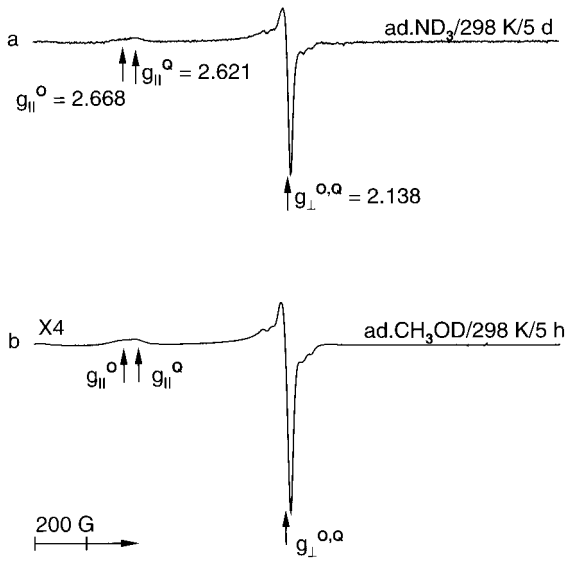

Figure 12. ESR spectra at 77 K of PdHK-SUZ-4 after (a) adsorption of 20 Torr ND_3 for 5 days, and (b) adsorption of 100 Torr CH_3OD for 5 h on a thermally reduced sample at 298 K.

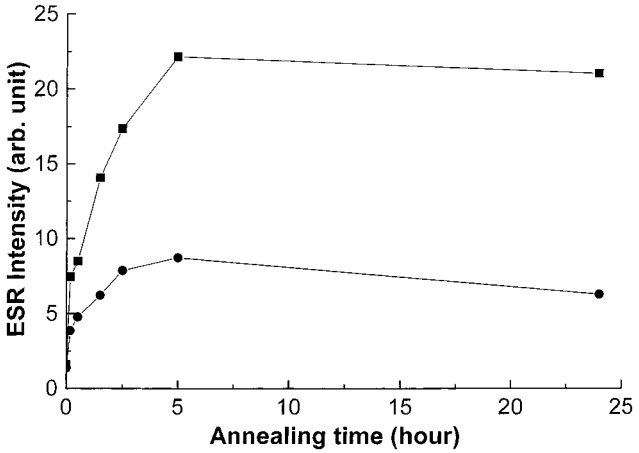

Figure 13. The changes in the ESR intensity of PdH-SUZ-4 as a function of annealing time after (a) adsorption of 100 Torr of CH_3OD for 5 h, and (b) adsorption of 20 Torr of dry H_2 on a thermally reduced sample at 298 K.

TABLE 2: ESR *g* Values of Paramagnetic Species Produced in PdH-Mordenite, PdH-Ferrierite, and PdHK-SUZ-4 after Reduction and Adsorbate Interactions

matrix	adsorbate	assignment	*g*// or g_1	*g*⊥ or g_2	g_3	species
PdH-mor	none	Pd(I)	2.976	2.207		A
PdH-mor	CH_3OD	Pd(I)−$(CH_3OD)_n$	2.799	2.140		B
PdH-mor	CH_3OD	Pd(I)−$(CH_3OD)_n$	2.704	2.140		C
PdH-mor	C_2D_4	Pd(I)−$(C_4D_8)_n$	2.675	2.077		D
PdH-mor	C_2D_4	Pd(I)−$(C_2D_4)_n$	2.419	2.038		E
PdH-fer	none	Pd(I)	2.645	2.136		H
PdH-fer	CH_3OD	Pd(I)−$(CH_3OD)_n$	2.539	2.137	2.105	I
PdH-fer	C_5D_5N	Pd(I)−$(C_5D_5N)_n$	2.410	2.059	2.023	J
PdH-fer	C_2D_4	Pd(I)−$(C_2D_4)_n$	2.412	2.053	2.019	L
PdH-fer	C_2D_4	Pd(I)−$(C_4D_8)_n$	2.655	2.079		M
PdH-fer	C_2D_4	Pd(I)−$(C_4D_8)_n$	2.272	2.049		N
PdHK-SUZ-4	none	Pd(I)	2.668	2.138		O
PdHK-SUZ-4	CO	Pd(I)−$(CO)_3$	2.198	2.044		P
PdHK-SUZ-4	NH_3	Pd(I)	2.621	2.138		Q
	CH_3OD	Pd(I)				Q
	C_2D_4	Pd(I)				Q

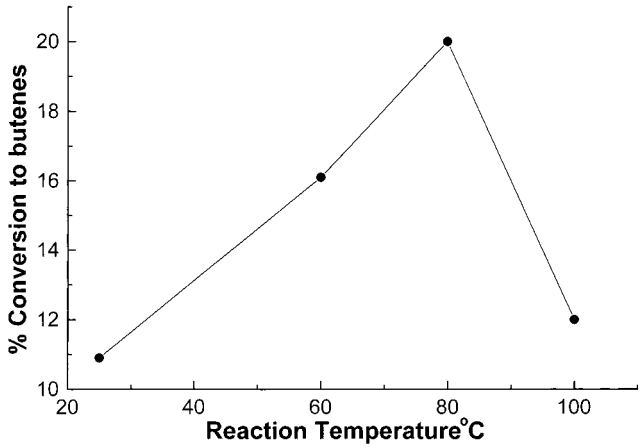

Figure 14. The percent of ethylene converted to *n*-butenes versus reaction temperature for PdH-clinoptilolite.

TABLE 3: Ethylene Dimerization and Equilibrium Distribution of *n*-Butenes in Palladium-Exchanged Clinoptilolite, Mordenite, Ferrierite, and SUZ-4

			distribution %		
catalyst	reaction temp/K	conversion %	1-butene	*cis*-2-butene	*trans*-2-butene
PdH-clino	298 K	10.9	5.7	24.8	69.8
	333 K	16.1	5.4	27.0	67.6
	353 K	20.3	5.4	28.4	66.2
	473 K	11.4	5.8	28.8	65.4
PdH-mor	353 K	6.3	11.1	36.1	52.8
PdH-fer	353 K	4.8	11.8	35.3	52.9
PdHK-SUZ-4	353 K	8.2	5.4	35.1	59.5

= 0.10). In comparison with PdH-ferrierite (5% conversion, Pd/Al = 0.36), PdHK-SUZ-4 (Pd/Al = 0.30) shows a higher ethylene dimerization activity of 8% conversion. In all cases the selectivity for the formation of *n*-butenes is close to 100%.

Figure 14 shows the percent conversion of ethylene to *n*-butenes as a function of the reaction temperature for PdH-clinoptilolite, which exhibits the highest activity for ethylene dimerization under the reaction condition. It is evident that the conversion percent increases as the reaction temperature increases from ~11% at 298 K to ~20% at 353 K but when the temperature exceeds 353 K, the dimerization activity decreases to reach 11% conversion to *n*-butenes at 473 K.

It has been reported that ethylene is initially dimerized to 1-butene, which is subsequently isomerized to *cis*-2-butene and *trans*-2-butene.[29] Table 3 shows the distribution of *n*-butenes in PdH-clinoptilolite, PdH-mordenite, PdH-ferrierite, and PdHK-SUZ-4 after a reaction time of 24 h at 353 K. PdH-clinoptililote and PdHK-SUZ-4 have similar thermal equilibrium distributions of *n*-butenes with *trans*-2-butene most abundant. For PdH-mordenite and PdH-ferrierite the relative amount of 1-butene in the gas phase is higher, indicating slower isomerization of 1-butene to *cis*- and *trans*-2 butene in these systems compared to clinoptilolite and SUZ-4.

Discussion

Thermal reduction of Pd(II) incorporated into four channel-type zeolites, H-clinoptilolite, H-mordenite, H-ferrierite, and HK-SUZ-4, generates single isolated Pd(I) with different ESR parameters. This single isolated Pd(I) is reproduced by hydrogen reduction of PdH-clinoptilolite, PdH-mordenite, and PdH-ferrierite at high temperature showing a higher ESR intensity, compared to that of Pd(I) observed by thermal reduction. The Pd(I) species found in mordenite, ferrierite, and SUZ-4 are axially symmetric while Pd(I) in clinoptilolite[14] has rhombic symmetry. These four zeolites show no big difference in the reducibility of Pd(II) upon thermal reduction.

The accessibility of Pd(I), based on the interaction with various sizes of adsorbates, is different in these four zeolites. A previous study concerning the nature and adsorbate interactions of Pd(I) in clinoptilolite[14] suggested that Pd(I) is located at a site which is not accessible to benzene and pyridine, probably a site within an 8-ring channel parallel to the main 10-ring channel of clinoptilolite, while molecules smaller than pyridine easily interact with Pd(I). Adsorption of methanol and pyridine on thermally reduced mordenite and ferrierite at room temperature leads to the formation of new ESR species due to Pd(I) complexes with methanol and pyridine. No remaining isolated Pd(I) species is observed in these materials after adsorption of methanol and pyridine, indicating a high accessibility to Pd(I) within the structures of mordenite and ferrierite. This suggests that Pd(I) is probably situated in a main 12-ring and 10-ring channel of mordenite and ferrierite, respectively.

PdH-mordenite and PdH-ferrierite also show some similarities upon adsorption of ethylene on thermally reduced samples. Our ESR results indicate that all Pd(I) ions completely interact with ethylene and form $Pd(I)-(C_2D_4)_n$ complexes after adsorption of ethylene at 298 K. These observations are consistent with the ESR results observed after adsorption of methanol and pyridine on PdH-mordenite and PdH-ferrierite, suggesting that Pd(I) ions occupy relatively accessible sites. As a result of Pd(I) interaction with ethylene for a longer time at 298 or 353 K, several ESR species assigned to Pd(I) complexes with butene are observed. Mordenite generates a single Pd(I)−butene complex along with a $Pd(I)-(C_2D_4)_n$ complex at 298 and 353 K while ferrierite produces two axial species due to Pd(I) complexes with butene only after annealing at 353 K.

The interaction of Pd(I) with various adsorbates is unique in PdHK-SUZ-4. The ESR intensity of Pd(I) species O formed by thermal reduction of PdHK-SUZ-4 is increased upon adsorption of dry hydrogen, ethylene, ammonia, and methanol at room temperature. The facts that no new ESR signal is observed after adsorption of these molecules on SUZ-4 and that Pd(I) species O increases with annealing time at room temperature indicate that these adsorbates reduce the remaining Pd(II) to Pd(I) in SUZ-4. A similar behavior has been observed in PdNaK-clinoptilolite[14] where Pd(II) located in a main 10-ring channel is reduced by methanol at room temperature. However, the stability of Pd(I) in clinoptilolite is different from that of Pd(I) in PdHK-SUZ-4, reflecting different locations of Pd(I) in these two materials. The Pd(I) formed in clinoptilolite was further reduced to Pd(0) clusters by direct interaction with methanol in the large 10-ring channels. Whereas, PdHK-SUZ-4 shows no broad isotropic ESR signal associated with the formation of Pd(0) clusters even after annealing for 24 h, indicating that Pd(II) responsible for the formation of Pd(I) species O is at a site within the small cages of SUZ-4 where Pd(I) is stablilized toward further reduction to Pd(0).

Adsorption of CO on thermally reduced Pd(I)HK-SUZ-4 gives more information about the location of palladium in the SUZ-4 structure. Pd(I) coordinates with three CO molecules to form a $Pd(I)-(CO)_3$ complex in the SUZ-4 structure. However, the observation of Pd(I) mostly remaining without interacting with CO suggests that Pd(I) in SUZ-4 is situated at a site which is less accessible to CO. The behavior of Pd(I) in SUZ-4 with respect to CO adsorption is different from the behavior in PdH-clinoptilolite, PdH-mordenite, and PdH-ferrierite where all the Pd(I) immediately coordinated with CO upon adsorption of CO

at 298 K. This again supports that Pd(I) species O produced in PdHK-SUZ-4 is located within the small cages formed with 5-rings and 6-rings. These cages are interconnected by double 6-ring windows that form 6-ring channels parallel to the main 10-ring channel of SUZ-4. In zeolites containing small cavities and channels, it is a common phenomenon that metal ions easily migrate from supercages and large channels to smaller ones during dehydration.[30] This is mainly due to the high negative charge density in the small cages and channels. It has been previously observed that metal ions initially located within the supercage of X and Y zeolites migrate to a smaller sodalite cage during the dehydration process.[5,6] Similarly, palladium ions in PdHK-SUZ-4 probably move to the small cages during dehydration where Pd(I) cannot coordinate with CO molecules.

Another new species Q is observed along with Pd(I) species O when samples anneal for a longer time after adsorption of molecules such as ammonia, ethylene and methanol. This species Q showing similar ESR parameters to those of Pd(I) species O is generated only after prolonged annealing time no matter what type of adsorbate is used. This suggests that species Q can be assigned to another isolated Pd(I) located at a site which is more difficult to be reduced compared to that of Pd(I) species O.

The formation of these stable isolated Pd(I) cannot be explained in terms of direct contact between Pd(II) and the adsorbate if Pd(II) is situated within a small cage of SUZ-4. The reduction of Pd(II) in a small cage of SUZ-4 could proceed via electron transfer through the zeolite framework at 298 K in the presence of adsorbates such as ethylene and methanol. A similar charge-transfer process was proposed for the reduction of Pd(II) by benzene at room temperature in PdNa-Y zeolite.[31,32] This unique behavior of SUZ-4 is closely associated with the structure of SUZ-4.

Even though SUZ-4 and ferrierite are structurally related zeolites, the behavior of PdHK-SUZ-4 with respect to various adsorbates is significantly different from that of PdH-ferrierite. The ESR results with various adsorbates indicate that Pd(I) in SUZ-4 is less accessible than in ferrierite and that the reduction of Pd(II) to Pd(I) occurs in SUZ-4 via indirect interaction with adsorbates except for hydrogen adsorption. These differences between PdHK-SUZ-4 and PdH-ferrierite are again attributed to a difference in the location and environment of Pd(I) in the two materials. The main structural difference between these two zeolites is the presence of small cages within the SUZ-4 structure.[21,22] We suggest that two Pd(I) species are located in the small cages in SUZ-4 but in different sites and environments where Pd(I) in one site is more difficult to reduce. Two cation sites have been previously identified within the small cages of SUZ-4 from single-crystal X-ray diffraction.[21] The most preferable cation site is the center of the small cage. The other site is at the center of a double 6-ring or hexagonal prism.

Ethylene is selectively dimerized to *n*-butenes on all these four Pd-containing zeolites, PdH-clinoptilolite, PdH-mordenite, PdH-ferrierite, and PdHK-SUZ-4, when ethylene is adsorbed on thermally reduced samples containing Pd(I) at room temperature followed by annealing at 353 K. The fact that no catalytic activity for ethylene dimerization is shown for materials not containing palladium ions and without a reduction pretreatment of Pd(II)-exchanged samples suggests that monovalent Pd(I) is the catalytically active site for ethylene dimerization. Ethylene dimerization activity has been studied in other nickel-exchanged and palladium-exchanged zeolites and SAPO materials.[11−13,33] The catalytic activity in these materials was affected by the amount, location, and accessibility of paramagnetic Ni(I) and Pd(I). These factors are equally relevant in PdH-clinoptilolite, PdH-mordenite, PdH-ferrierite, and PdHK-SUZ-4. The activity for the formation of *n*-butene is higher in PdH-clinoptilolite than in PdH-ferrierite when they have the same Pd/Al ratio. This difference is probably explained by the different location of Pd(I) in clinoptilolite and mordenite since there is no big difference in the reducibility of Pd(II) in clinoptilolite and mordenite. Pd(I) located in a main 12-ring channel of mordenite deactivates faster than Pd(I) in an 8-ring channel of clinoptilolite. This result is consistent with the formation of stable Pd(I)$-(C_2H_4)_n$ complexes even at 353 K in clinoptilolite. On the other hand, the higher turnover in PdHK-SUZ-4 is somewhat surprising since the ESR results show that no Pd(I) complex with ethylene is observed upon ethylene adsorption but is consistent with the trend that Pd(I) increases as the annealing time increases at 353 K. This also explains the higher activity of ethylene dimerization in PdHK-SUZ-4 than in PdH-ferrierite.

All these catalysts are found to deactivate for a longer reaction time due to the further reduction of active Pd(I) to inactive Pd(0) by ethylene and butene. The deactivation process has been previously reported to be greater for Pd(I) located at a more accessible site and at higher reaction temperature.[33,34] This is the possible reason the conversion ratio of ethylene to *n*-butenes in clinoptilolite drops at temperatures higher than 353 K.

Conclusions

The catalytic activity for ethylene dimerization is compared in four palladium-exchanged zeolites with different channel systems, including PdH-clinoptilolite, PdH-mordenite, PdH-ferrierite, and PdHK-SUZ-4, by using a static reactor and gas chromatography. ESR spectroscopy is also used to study the location and accessibility of active Pd(I) which is required to understand the catalytic function of Pd(I) in the zeolite structure. Thermal and hydrogen reduction produce isolated Pd(I) in clinoptilolite, mordenite, ferrierite, and SUZ-4 with somewhat different ESR parameters. The interaction of Pd(I) with various sizes of adsorbates shows some similarities between PdH-mordenite and PdH-ferrierite but shows an unique difference in PdHK-SUZ-4.

For PdH-mordenite and PdH-ferrierite, Pd(I) immediately coordinates with adsorbates such as methanol, ethylene, and pyridine to give the corresponding complexes, indicating that Pd(I) in mordenite and ferrierite is situated in main 12-ring and 10-ring channels, respectively. On the other hand, the ESR intensity of Pd(I), which is formed by thermal reduction of PdHK-SUZ-4, is increased without forming a complex with adsorbates no matter what type of adsorbate is added and another Pd(I) species is produced at a later stage. These two Pd(I) species are located at two different sites in SUZ-4, probably within the small cages where one site is more difficult to reduce than the other. The observation of Pd(I) mostly remaining after adsorption of CO on SUZ-4 further supports that the Pd(I) produced after thermal reduction is located in the small cages. This is consistent with the highest stability and the least accessibility to Pd(I) observed in SUZ-4 compared to Pd(I) in clinoptilolite, mordenite, and ferrierite.

The catalytic results indicate that ethylene dimerization occurs on Pd(I) in ion-exchanged clinoptilolite, mordenite, ferrierite, and SUZ-4, as expected by the ESR results observed after adsorption of ethylene on thermally reduced samples followed by annealing at 298 and 353 K. The activity for formation of butene is higher in PdH-clinoptilolite where Pd(I) is located in a site within a 8-ring channel compared that observed in PdH-

mordenite where Pd(I) is situated at a more accessible site, in a 12-ring channel. The high turnover in PdHK-SUZ-4 is consistent with an increase in Pd(I) with annealing time of an ethylene-adsorbed sample at 353 K. All these four catalysts deactivate at a longer reaction time, probably due to further reduction of active Pd(I) to inactive Pd(0) by ethylene and butene.

Acknowledgment. This research was supported by the U.S. National Science Foundation, the Robert A. Welch Foundation, the Environmental Institute of Houston, and the Korea Science and Engineering Foundation through the Advanced Materials Research Center for a Better Environment at Taejon National University of Technology.

References and Notes

(1) Dyer, A. *An Introduction to Zeolite Molecular Sieves*; Wiley: Chichester, 1988; p 117.
(2) Chen, N. Y.; Garwood, W. E.; Dwyer, F. G. *Shape Selective Catalysis in Industrial Application*; Marcel Dekker: New York, 1996.
(3) Kazansky, V. B.; Elev, I. V.; Shelimov, B. N. *J. Mol. Catal.* **1983**, *21*, 265.
(4) Oliver, D.; Richard, M.; Che, M.; Bonson-Verduraz, F.; Clarkson, R. B. *J. Phys. Chem. B* **1980**, *84*, 420.
(5) Michalik, J.; Heming, M.; Kevan, L. *J. Phys. Chem.* **1986**, *90*, 2132.
(6) Ghosh, A. K.; Kevan, L. *J. Phys. Chem.* **1990**, *94*, 1953.
(7) Yu, J. S.; Kurshev, V.; Kevan, L. *J. Phys. Chem.* **1994**, *98*, 10225.
(8) Den Ouden, C. J. J.; Jackson, R. A.; Catlow, C. R. A.; Post, M. F. M. *J. Phys. Chem.* **1990**, *94*, 5286.
(9) Azuma, N.; Kevan, L. *J. Phys. Chem.* **1995**, *99*, 5083.
(10) Azuma, N.; Hartmann, M.; Kevan, L. *J. Phys. Chem.* **1995**, *99*, 6670.
(11) Ghosh, A. K.; Kevan, L. *J. Phys. Chem.* **1988**, *92*, 4439.
(12) Ghosh, A. K.; Kevan, L. *J. Phys. Chem.* **1990**, *94*, 3117.
(13) Hartmann, M.; Kevan, L. *J. Phys. Chem.* **1996**, *100*, 4606.
(14) Choo, H.; Prakash, A. M.; Zhu, Z.; Kevan, L. *J. Phys. Chem.* **2000**, *104*, 3608.
(15) (a) Wise, W. S.; Tschernich, R. W. *Am. Mineral*. **1976**, *61*, 60. (b) Whittemore, O. J. *Am. Mineral*. **1972**, *57*, 1146.
(16) Meier, W. M.; Olson, D. H. *Atlas of Zeolite Structure Types*, 3rd ed.; Butterworth−Heinemann: London, 1992.
(17) Koyama, Y.; Takeuchi, Y. Z. *Kristallogr*. **1997**, *145*, 216.
(18) Shiokawa, K.; Ito, M.; Itabashi, K. *Zeolites* **1989**, *9*, 170.
(19) Vaughan, P. A. *Acta Crystallogr*. **1966**, *21*, 983.
(20) Barri, S. I. U.S. Patent 5,118,483, 1992.
(21) Lawton, S. L.; Bennett, J. M.; Schlenker, J. L. Rubin, M. K. *J. Chem. Soc., Chem. Commun.* **1993**, 894.
(22) Lukyanov, D. B.; Zholobenko, V. L.; Dwyer, J.; Barri, S. I.; Smith, W. J. *J. Phys. Chem. B* **1999**, *103*, 197.
(23) Choo, H.; Hong, S. B.; Kevan, L. *J. Phys. Chem. B* **2001,** *105*, 0000.
(24) Kim, T. J.; Ahn, W. S.; Hong, S. B. *Microporous Mater*. **1996**, *7*, 35.
(25) Paik, W. C.; Shin, C. H.; Hong, S. B. *J. Chem. Soc., Chem. Commun.* **2000**, 1609.
(26) Schoonheydt, R. A.; Roodhooft, D. *J. Phys. Chem.* **1986**, *90*, 6319.
(27) Prakash, A. M.; Wasowicz, T.; Kevan, L. *J. Phys. Chem. B* **1997**, *101*, 1985.
(28) Yu, J. S.; Kevan, L. *J. Chem. Soc., Faraday Trans.* **1995**, *91*, 3987.
(29) Sohn, J. R.; Shin, D. C. *J. Catal.* **1996**, *160*, 314.
(30) Sachtler, W. M. H.; Zhang, Z. *Adv. Catal.* **1993**, *39*, 129.
(31) Bergeret, G.; Tran Manh Tri; Gallezot, P. *J. Phys. Chem.* **1983**, *87*, 1160.
(32) Romanikov, V. N.; Ione, K. G.; Pederson, L. A. *J. Catal.* **1980**, *66*, 121.
(33) Hartmann, M.; Kevan, L. *J. Chem. Soc., Faraday Trans.* **1996**, *92*, 1429.
(34) Coughlan, B.; Keane, M. A. *J. Catal.* **1990**, *123*, 264.